IJIE

INTERNATIONAL JOURNAL OF INTEGRATED ENGINEERING
ISSN: 2229-838X e-ISSN: 2600-7916

Vol. 18 No. 1 (2026) 229-241
https://publisher.uthm.edu.my/ojs/index.php/ijie

Mitigation of LFOs within Smart Grid Using Adaptive Fuzzy Logic Neural Network Control Scheme

Nadia Zeb[1], Shamsul Aizam Zulkifli[1]*, Muhamad Syazmie Sepeeh[2], Nedim Tutkun[3], Noor Hisyam Ibrahim[4]

[1] *Faculty of Electrical and Electronic Engineering, Universiti Tun Husein Onn Malaysia, 86400, Johor, MALAYSIA*
[2] *Department of Electrical and Electronic Engineering, MAHSA University. Jenjarom, 42610, Selangor, MALAYSIA*
[3] *Department of Electrical and Electronic Engineering, Istanbul Ticaret University, 34840, Istanbul TÜRKIYE*
[4] *Rocksolid Technology Solutions Sdn Bhd, Universiti Putra Malaysia (UPM) D-G-6, UPM-MTDC Technology Center III, 43400, Seri Kembangan, Selangor, MALAYSIA*

*Corresponding Author: aizam@uthm.edu.my
DOI: https://doi.org/ 10.30880/ijie.2026.18.01.017

Article Info

Received: 1 January 2026
Accepted: 30 March 2026
Available online: 20 April 2026

Keywords

Low-frequency oscillations, smart grid, Generalized Unified Power Flow Controller, Flexible AC Transmission System, adaptive fuzzy logic neural network controller, renewable energy resources

Abstract

Power system stability is challenged by low inertia and Low-Frequency Oscillations (LFOs) within 0.1–2 Hz. Short-circuit faults occurring within milliseconds can cause generator desynchronization. Reducing LFOs under stress improves stability and power transfer control, which is vital for inter-regional power exchange. Based on third-generation devices from the Flexible AC Transmission System (FACTS), this study introduces a Smart Grid (SG) control strategy that emphasizes the Generalized Unified Power Flow Controller (GUPFC) combined with an adaptive auxiliary control scheme. A centralized, real-time supplementary controller is developed to mitigate low-frequency oscillations (LFOs), enhance effective system inertia, and optimize power flow. A quantitative evaluation of the proposed approach performance in per unit (p.u.), demonstrates measurable reductions in oscillations and noticeable improvements in system inertia. The proposed Adaptive Fuzzy Logic Neural Network Controller (AFLNNC) mitigates oscillations up to 15-25%, enhances dynamic performance, reduces DC capacitor voltage fluctuations by 20%, and stabilizes bus voltage magnitude within 5% of the nominal values. Synchronous and asynchronous generators, grid-to-vehicle systems, renewable energy sources (wind, photovoltaic), and residential loads are all included in the two-area test system. The sever $3\varphi - g$ faults in the Smart Grid are modeled and validated using MATLAB/Simulink simulations. The AFLNNC proves to be a powerful and intelligent strategy for boosting the secure and stable system for future renewable-dominated power systems.

1. Introduction

The integration of renewables with the grid has become a top priority, thanks to their abundance and environmental benefits. However, their inherently variable output challenges introduce stochastic dynamic characteristics, reduction in system inertia [1], and low-frequency oscillations (LFOs) in the 0.1–2 Hz range [2] [3]. Essential to control these power fluctuations while demand is continuously fluctuating to maintain constant voltage and frequency and guarantee a steady, dependable, and uninterrupted supply of electricity. Diverse solutions, such as solar, wind, and electric vehicles (EVs), are being adopted to meet growing energy demands [4]. In the meantime, centralized, distributed, or decentralized Smart Grid (SG) architectures provide more secure power transfer, improved reliability, and flexible designs.

However, grid integration of renewables exacerbates problems such as power swings, harmonic distortion, voltage excursions, and stability degradation, all of which need to be considered when modelling the nonlinear dynamics of the SG [5]. Protection, monitoring, and security are made more difficult when synchronous and asynchronous machines are combined [6]. Frequency deviations brought on by abrupt changes in load, converter switching, or fault events are amplified by the reduced inertia from photovoltaics, wind farms, and electric vehicles [7]. Despite having an acceptable frequency range of 0.1–2 Hz, inter-area LFOs between large generating areas have the potential to disrupt stable energy transfers unless they are actively damped [8].

A versatile solution to these problems is offered by power electronic converter-based controller such as Flexible AC Transmission System (FACTS). To improve load loading, the Unified Power Flow Controller (UPFC) provides combined series-and-shunt converter control [9] **.** The two different Voltage Source Converters (VSCs) installed in series on two different lines with a common VSC connected in shunt via a DC-link capacitor, the third generation advanced Generalized Unified Power Flow Controller (GUPFC) expands this idea [10]. Five degrees of freedom are provided by the GUPFC to control power flows, phase angles, reactance, and line voltages across several transmission lines [11]. Compared to the UPFC, this extra flexibility allows for more efficient torque mitigation, power control, speed regulation, and transient stabilization.

Many control strategies have been examined to make use of FACTS devices during disturbances. For instance, ant-lion optimization adjusted a UPFC equipped power system stabilizer for quick stabilization [12]. An interline power-flow controller with LMI-based damping used the PONY algorithm to reduce oscillation [13]. A wide area damping controller (WADC), although complicated, improved inertia response through modified particle swarm optimization [14]. Time-delay feedback control has dealt with uncertainties from large-scale renewables [15]. Additionally, adaptive neuro-fuzzy schemes have actively countered oscillations and nonlinearities.

Despite these advances, the highly nonlinear behaviour of Renewable Energy Sources (RES) integrated grids demands more robust, adaptable damping mechanisms. In response, proposed an Adaptive Fuzzy Logic Neural Network Controller (AFLNNC). An AFLNNC is an adaptive control that combines human-like fuzzy reasoning with neural network adaptation and the learning algorithm. The tuning of parameters is based on system feedback. The layered structure allows the controller to adapt to changing system dynamics without requiring a precise mathematical model. The FLC's linguistic rules approximate complex mappings, while the ANN updates its weights in real time to reflect evolving grid conditions. An adaptive design reduces computational complexity, accelerates simulation runtimes, and offers resilient, model-free damping of LFOs. The application of a third-generation GUPFC to multi-line scenarios in RES-rich grids, and the development of an online AFLNNC supplementary controller for improved oscillation damping and stability.

Although there are different control strategies for FACTS devices, more robust and flexible damping methods would be necessary, given the variables and nonlinear characteristics of high renewable energy penetration grids. Most of the current approaches, like ant-lion optimization, LMI-based damping, and particle swarm approach only address uncertainties or are required to have complex design. There is, however, still a demand for model-free and adaptive control approaches that can learn directly from system feedback in real-time to accommodate changing grid conditions. AFLNNCs using advanced multi–terminal FACTS devices for oscillation damping and stability improvement in renewable-integrated smart grids have not been extensively explored. That suggests there is a need for intelligent and adaptive control strategies that can contribute toward ensuring reliable grid performance in systems having a significant amount of renewable energy integrated into them using rule-based reasoning combined with learning capability.

The primary objective of this research is to enhance the stability of smart grid systems and mitigate oscillations through the effective integration of renewable energy sources. To achieve this objective, AFLNNC in coordination with a GUPFC has been designed and implemented. The proposed control framework is intended to improve the dynamic performance of the system by addressing the challenges introduced by high renewable energy penetration, thereby contributing to a more stable and reliable smart grid operation. In various operational scenarios, including fault events, load fluctuations, and nonlinear characteristics related to renewable generating units, the integrated controller will help maintain stable power transfer, enhance transient responses, and effectively dampen oscillations. This study places a strong emphasis on modeling systems as well as designing controllers and evaluating performance for a renewable-rich smart grid network. There will also be emphasis placed on damping inter-area oscillations and providing transient stability and regulation of power flows. Research is done through simulation on a MATLAB/Simulink platform and will extend up to 24 hours to evaluate steady state and dynamic response to different operating conditions.

Here are the sections of this paper: Section two presented the methods for integrating the GUPFC with the smart grid model. In Section three provide the mathematical model of the Adaptive Fuzzy Logic Neural Network Controller. In Section four discusses the simulation results of a $3\varphi - g$ fault. Lastly, conclusion is discussed in Section five.

2. Integration of GUPFC on SG model

A diagram depicting a single line of an SG system, where Area 1 produces 10600MW and Area 2 generates 10000MW of power, is presented in Fig 1.

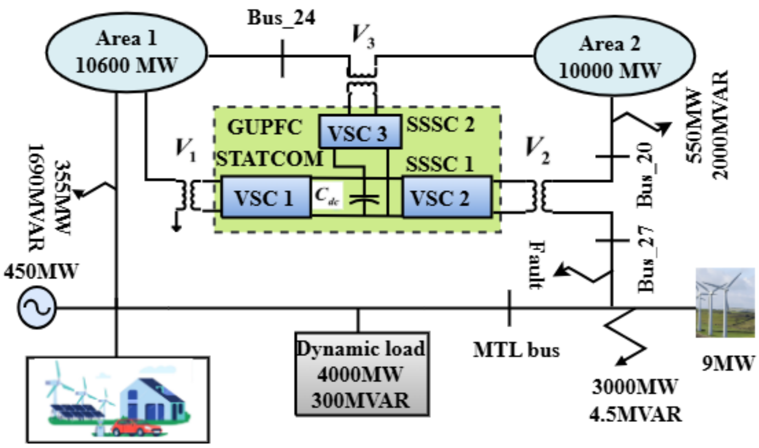

Fig. 1 *Single-line diagram of the proposed smart grid system*

The 25 MW renewable energy system is made up of an electric vehicle (EV) plant, a wind farm, and a photovoltaic (PV) power plant. There are four generators in Area 1 and two in Area 2, respectively. Seven generators linked to a 735 kV transmission network with a transmission line voltage of 13.8 kV make up the entire energy system. With a generator output voltage of 13.8 kV in kilovolt units, the total energy production is measured in megawatts.

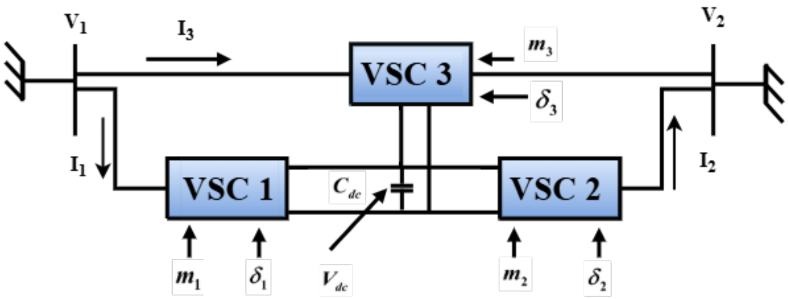

Fig. 2 *GUPFC block diagram*

One shunt converter (VSC 1) and two series converters (VSC 2 and VSC 3) make up the GUPFC [16]. A gate signal activates the three-phase voltage source converter (VSC). To enable the bidirectional flow of power between the VSC converters, a DC link capacitor called C_{dc} is positioned between them [17]. The modulation indices (m) and gate-triggered phase angles (δ) of the series and shunt-connected VSC converters, which are defined as (m_1, m_2, m_3), and $(\delta_1, \delta_2, \delta_3)$ respectively, are the six input control signals that the GUPFC uses to function [18]. The operation of GUPFC on the transmission line is described Fig 2. Equations (1)– (3) represent the three-phase dynamic differential equations. equations for the three-phase dynamics after transients and transformer resistance are ignored.

$$\begin{bmatrix} \frac{dI_{1a}}{dt} \\ \frac{dI_{1b}}{dt} \\ \frac{dI_{1c}}{dt} \end{bmatrix} = \begin{bmatrix} -\frac{r_1}{l_1} & 0 & 0 \\ 0 & -\frac{r_1}{l_1} & 0 \\ 0 & 0 & -\frac{r_1}{l_1} \end{bmatrix} \begin{bmatrix} I_{1a} \\ I_{1b} \\ I_{1c} \end{bmatrix} - \frac{m_1 v_{dc}}{2l_1} \begin{bmatrix} \cos(wt+\delta_1) \\ \cos(wt+\delta_1-120^\circ) \\ \cos(wt+\delta_1+120^\circ) \end{bmatrix} + \begin{bmatrix} \frac{1}{l_1} & 0 & 0 \\ 0 & \frac{1}{l_1} & 0 \\ 0 & 0 & \frac{1}{l_1} \end{bmatrix} \begin{bmatrix} V_{1ta} \\ V_{1tb} \\ V_{1tc} \end{bmatrix} \tag{1}$$

$$\begin{bmatrix} \frac{dI_{2a}}{dt} \\ \frac{dI_{2b}}{dt} \\ \frac{dI_{2c}}{dt} \end{bmatrix} = \begin{bmatrix} -\frac{r_2}{l_2} & 0 & 0 \\ 0 & -\frac{r_2}{l_2} & 0 \\ 0 & 0 & -\frac{r_2}{l_2} \end{bmatrix} \begin{bmatrix} I_{2a} \\ I_{2b} \\ I_{2c} \end{bmatrix} - \frac{m_2 v_{dc}}{2l_2} \begin{bmatrix} \cos(wt+\delta_2) \\ \cos(wt+\delta_2-120^\circ) \\ \cos(wt+\delta_2+120^\circ) \end{bmatrix} + \begin{bmatrix} \frac{1}{l_2} & 0 & 0 \\ 0 & \frac{1}{l_2} & 0 \\ 0 & 0 & \frac{1}{l_2} \end{bmatrix} \begin{bmatrix} V_{2ta} \\ V_{2tb} \\ V_{2tc} \end{bmatrix} \tag{2}$$

$$\begin{bmatrix} \frac{dI_{3a}}{dt} \\ \frac{dI_{3b}}{dt} \\ \frac{dI_{3c}}{dt} \end{bmatrix} = \begin{bmatrix} -\frac{r_3}{l_3} & 0 & 0 \\ 0 & -\frac{r_3}{l_3} & 0 \\ 0 & 0 & -\frac{r_3}{l_3} \end{bmatrix} \begin{bmatrix} I_{3a} \\ I_{3b} \\ I_{3c} \end{bmatrix} - \frac{m_3 v_{dc}}{2l_3} \begin{bmatrix} \cos(wt+\delta_3) \\ \cos(wt+\delta_3-120^\circ) \\ \cos(wt+\delta_3+120^\circ) \end{bmatrix} + \begin{bmatrix} \frac{1}{l_3} & 0 & 0 \\ 0 & \frac{1}{l_3} & 0 \\ 0 & 0 & \frac{1}{l_3} \end{bmatrix} \begin{bmatrix} V_{3ta} \\ V_{3tb} \\ V_{3tc} \end{bmatrix} \tag{3}$$

The transmission line's resistance is denoted by r, its inductance by l, and its phase angle with respect to phases a, b, and c by. Whereas the phase angle of the gearbox line compensates for the series, the voltage applied in series with the gearbox line compensates for the shunt. The voltage in relation to the line's angle modifies the active energy (P) transmitted through the line, whereas the magnitude of the voltage m modifies the reactive energy (Q) [19]. Reactive energy is stored in a capacitor known as C_{dc}, which is connected to the shunts and series converters.

With converters, the DC coupling capacitor regulates the active energy while preserving the reactive energy throughout the capacitor [11]. The purpose of the AC voltage control loop and other DC voltage control mechanisms is to stabilize the DC coupling voltage at a predetermined level and regulate the voltage range [16]. Reactive energy affects the AC transmission line's voltage range when it is in shunting mode. The real power (P) transferred through the DC link depends on the phase angle difference between the sending-end voltage (V_1) and the receiving-end voltage (V_2). To lower the errors at steady state, the series converter senses, regulates, and modifies the P and Q values.

The mathematical model of the generator is represented from equation (4)- (7). The dynamic machine equation is expressed as in dq − axis [20]:

$$\dot{w} = \frac{1}{H}\left[P_m - P_e - D\Delta w\right], \tag{4}$$

$$\dot{\boldsymbol{E}}'_q = \frac{\boldsymbol{1}}{\boldsymbol{T}'_{d0}}\left[-\boldsymbol{E}_q + \boldsymbol{E}_{fd}\right], \tag{5}$$

$$\Delta\dot{\boldsymbol{E}}_{fd} = \frac{\boldsymbol{1}}{\boldsymbol{T}_A}\left[\boldsymbol{K}_A(\boldsymbol{V}_{t0} - \boldsymbol{V}_t) - \Delta\boldsymbol{E}_{fd}\right], \tag{6}$$

$$\dot{V}_{dc} = \frac{m_1}{2C_{dc}}\left[I_{1d}\cos\delta_1 + I_{1q}\sin\delta_1\right] + \frac{m_2}{2C_{dc}}\left[I_{2d}\cos\delta_2 + I_{2q}\sin\delta_2\right] + \frac{m_3}{2C_{dc}}\left[I_{3d}\cos\delta_3 + I_{3q}\sin\delta_3\right] \tag{7}$$

$$P_e = v_q i_q + v_d i_d, E_q = E_q' + (x_d - x_d')i_d, v_q = E_q' - x_d i_d, \tag{8}$$

$$v_d = x_d i_d, v_t = \sqrt{(v_d^2 + v_q^2)}, i_d = i_{1d} + i_{2d} + i_{3d}, \; i_q = i_{1q} + i_{2q} + i_{3q} \tag{9}$$

Here, D represents the damping coefficient, and H denotes the inertia constant. The synchronous speed of the generator is indicated by ω_0, while ω and δ correspond to the rotor speed and rotor angle, respectively. The mechanical input power and electrical output power of the generator are represented by P_{m} and P_{e}. The internal generated voltage, excitation voltage, and terminal voltage are denoted by $\dot{E}_q, E_{fd}$ and V_t respectively. Additionally, T_A represents the exciter time constant, K_A is the exciter gain, and $\acute{T}_{d0}$ denotes the open-circuit field time constant. The operation of the GUPFC controller is explained in Fig 3.

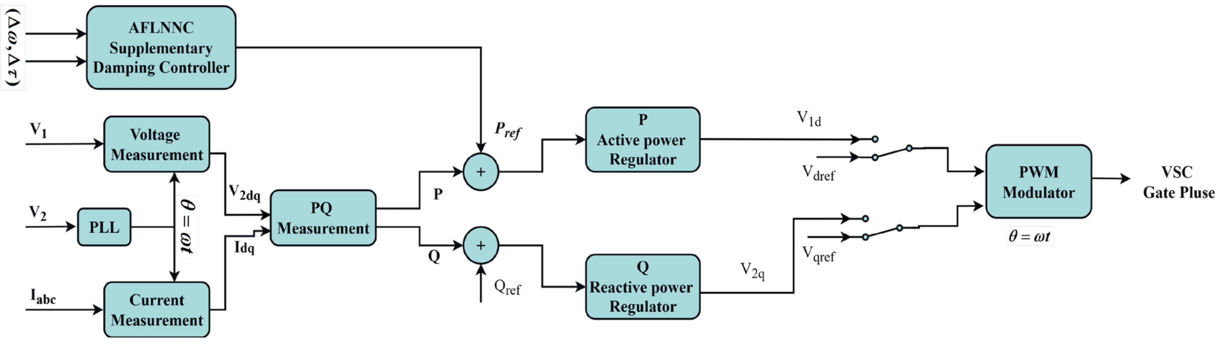

Fig 3 *Working of supplementary control with series compensator*

The behaviour of DC link voltage for GUPFC is determined using Kirchhoff's current law (KCL) method as shown in [21], represented by the equation (1), (2). and (3). The currents I_1, I_2, and I_3 represent the dq-axis currents of the VSC shunt and series converters. In developing the dynamic three-phase model of the GUPFC, the transformer resistance is neglected to simplify the analysis.

$$\begin{bmatrix} V_{1Td} \\ V_{1Td} \end{bmatrix} = \begin{bmatrix} 0 & -X_1 \\ X_1 & 0 \end{bmatrix} \begin{bmatrix} I_{1d} \\ I_{1q} \end{bmatrix} + \begin{bmatrix} \dfrac{m_1 \cos \delta_1 V_{dc}}{2} \\ \dfrac{m_1 \sin \delta_1 V_{dc}}{2} \end{bmatrix}, \tag{10}$$

$$\begin{bmatrix} V_{2Td} \\ V_{2Td} \end{bmatrix} = \begin{bmatrix} 0 & -X_2 \\ X_2 & 0 \end{bmatrix} \begin{bmatrix} I_{2d} \\ I_{2d} \end{bmatrix} + \begin{bmatrix} \dfrac{m_2 \cos \delta_2 V_{dc}}{2} \\ \dfrac{m_2 \sin \delta_2 V_{dc}}{2} \end{bmatrix}, \tag{11}$$

$$\begin{bmatrix} V_{3Td} \\ V_{3Td} \end{bmatrix} = \begin{bmatrix} 0 & -X_3 \\ X_3 & 0 \end{bmatrix} \begin{bmatrix} I_{3d} \\ I_{3q} \end{bmatrix} + \begin{bmatrix} \dfrac{m_3 \cos \delta_3 V_{dc}}{2} \\ \dfrac{m_3 \sin \delta_3 V_{dc}}{2} \end{bmatrix}, \tag{12}$$

Where X_1 is the reactance of the shunting transformer, X_2 and X_3 are respectively the reactance's of the series transformer. V_{dc} is the voltage through the DC capacitor according to the following formula [21]. $\boldsymbol{V_1}$ represents the output voltage of the shunt converter (VSC1), while V_2 and V_3 correspond to the output voltages of the series converters (VSC2 and VSC3). These voltages are used to formulate the standard linear model and its corresponding state-space representation as

$$\Delta\dot{x} = A\Delta x + B\Delta u, \tag{13}$$

where A is the plant model input state matrix and B is the GUPFC state input system matrix that help to find the eigenvalues to test open loop stability and controllability of the system as in reference [22]. The x input states vector and u is the output control vector.

$$x = [\Delta\delta \; \Delta w \; \Delta\dot{E}_q' \; \Delta E_{fd} \; \Delta V_{dc}], \tag{14}$$

$$u = [\Delta m_1\ \Delta\delta_1\ \Delta m_2\ \Delta\delta_2\ \Delta m_3\ \Delta\delta_3\ ], \tag{15}$$

Table 1 represents the variation in modulation indices (**m**) and gate-triggered phase angles (δ) of the Voltage Source Converter (VSC) system under different operating conditions, i.e., pre-fault, during fault, and post-fault. Shunt Converter (VSC 1) under pre-fault conditions, the modulation index of 0.8 with a phase angle =0, ensuring normal system operation. During fault, the modulation index significantly drops to 0.001, while the phase angle shifts negatively to -1.21 indicating the converter's response to suppress fault currents. Post-fault, the modulation index recovers close to the pre-fault value (0.78), while the phase angle stabilizes near zero restoring normal operation. VSC 2 converter initially, the modulation index was 0.77 with a phase angle of −1.96.

Table 1 *VSC gate trigger indices*

VSC converters	Gate trigger pulses	Pre Fault	During Fault	Post Fault
Shunt Converter	m_1	0.8	0.001	0.78
	δ_1	0	-1.21	-0.007
Series Converter 1	m_2	0.77	0.79	0.5
	δ_2	-1.96	2.653	2.66
Series Converter 2	m_3	0.5	0.426	0.48
	δ_3	2.47	3.13	2.25

The modulation index slightly increases during fault to 0.79, while the phase angle undergoes a significant positive shift to 2.653, showing active compensation to support voltage stability. The modulation index decreases to 0.5, while the phase angle remains almost constant around 2.66, ensuring steady-state recovery. In case of series converter 2 (VSC 3) the modulation index starts at 0.5 with a phase angle of 2.47. During fault, the modulation index decreases to 0.426, while the phase angle increases to 3.13, reflecting dynamic control during disturbance. Post-fault, both values move toward stability with m3=0.48 δ3=2.25.

3. An Adaptive Fuzzy Logic Neural Network Controller

An adaptive fuzzy logic neural network control is an advanced system that merges the learning abilities of neural networks with the reasoning skills of fuzzy logic [23]. It effectively incorporates fuzzy systems into the neural network's structure to process imprecise, ambiguous, or uncertain information [24]. The design of an AFLNNC generally consists of multiple layers, namely the input layer, hidden layer, and output layer. The input layer contains crisp values that are transformed into fuzzy sets using Gaussian membership functions. The network acquires knowledge by modifying the parameters of the fuzzy membership functions and rule weights based on training data, utilizing techniques such as gradient descent [25]. Fuzzy rules, which emulate human-like reasoning, can either be established prior to training or learned directly from data, enabling adaptability in the system. By managing system uncertainty according to input data, the FLC can reason similarly to humans while benefiting from the learning and adaptability of neural networks, making the proposed system intelligent and capable of effectively tackling complex challenges within power systems.

3.1 Input layer

The input variables $\tau\ and\ \omega$ is given to proposed controller. The aggregate function $g^k(.)$ links the nodes for inputting data [25].

$$input = g^k(x^k; W^k), \tag{16}$$

x^k is the input, W^k is the connection weights and g^k provides the input node.

$$output = O_i^k = f^k(g^k), \tag{17}$$

where f^k is the activation function of its input and O_i^k is the output layer. K represents the number of layers and "i" means the iteration term.

Int. Journal of Integrated Engineering Vol. 18 No. 1 (2026) p. 229-241

3.2 Layer 1

Input layer 1 directly transmit numerical inputs to the nest layer, here weights are considering unity by default, no weights are adjusted.

$$input = g_j^1\left(x^1; W_{ij}^1\right) = W_{ij}^1.x_i^1, \tag{18}$$

$$O_{ij}^1 = g_j^1\left(x_i^1; W_{ij}^1\right), \tag{19}$$

3.3 Layer 2 Fuzzification

Here gaussian membership function is used as fuzzy linguistic terms. The mean m and variance σ of fuzzy MF varies to adjust weights [26].

$$g_{ij}^2\left(x_i^2; W_{ij}^2\right) = g_{ij}^2\left(x_i^2;\ m_{ij}, W_{ij}^2\right) = -\frac{\left(x_{ij}^2 - m_{ij}\right)^2}{\sigma_{ij}^2} \tag{20}$$

$$O_{ij}^2 = exp\left[-\frac{\left(x_{ij}^2 - m_{ij}\right)^2}{\sigma_{ij}^2}\right], \tag{21}$$

m_{ij} is the mean and σ_{ij}^2 is the variance, and the 2 represents the number of layers. Update layer 2 weights after initialization of m and σ. Adjust mean its Mean and Sigma of Gaussian membership function automatically once initialized by

$$-\frac{\partial E}{\partial m_{ij}} = -\frac{\partial E}{\partial g_j^3}.\frac{\partial g_j^3}{\partial O_{ij}^2}\frac{\partial O_{ij}^2}{\partial m_{ij}}, \tag{22}$$

$$-\frac{\partial E}{\partial m_{ij}} = -\frac{\partial E}{\partial g_j^3}.\frac{\partial g_j^3}{\partial O_{ij}^2}\frac{\partial O_{ij}^2}{\partial m_{ij}}, \tag{23}$$

Then, update rules for m_{ij} and σ_{ij}

$$m_{ij}(K+1) = m_{ij}(k) + \eta_m.O_{ij}^2.\frac{2(x_{ij}^2 - m_{ij})}{O_{ij}^2} + \alpha_m.\Delta m_{ij}(k), \tag{24}$$

$$\sigma_{ij}(K+1) = \sigma\sigma_{ij}(k) + \eta_\sigma.O_{ij}^2.\frac{2(x_{ij}^2 - \sigma_{ij})^2}{O_{ij}^2} + \alpha_\sigma.\Delta\sigma_{ij}(k), \tag{25}$$

where η_m and η_σ are the learning rates and the momentum parameter for adjusting mean and sigma respectively.

3.4 Layer 3 Rule Layer

The antecedent matching and product operation is performed in layer 3.

$$g_{ij}^3\left(x_i^3; W_{ij}^3\right) = \Pi_{i=1}^n\left(x_i^3; W_{ij}^3\right), \tag{26}$$

$$O_{ij}^3 = g_j^3\left(x_i^3; W_{ij}^3\right), \tag{27}$$

for no weights adjusted here. The weights of layer 2 are adjusted, in layer 3 rules are defined after initiation of AFLNNC [27]. Rules are updated according to equation (21).

$$\delta_j^3 = -\frac{\partial E}{\partial g_i^3} = \Sigma_{j=1}^p(\delta_j^4.W_{ij}^4), \tag{28}$$

δ_j^3 is the error signal and P is the number of output nodes.

3.5 Layer 4 Defuzzification

Layer 4 performs the defuzzification to get the numerical output. The W_{ij}^4 is the connection weights between the ith rule node and the jth output node. The Center of Addition technique defuzzification technique is used to get the output node.

$$g_{ij}^4\left(x_i^4; W_{ij}^{34}\right) = \Sigma_{i=1}^{n}\left(x_i^4; W_{ij}^4\right), \tag{29}$$

$$O_j^4 = \frac{g_j^4(x_i^4; W_{ij}^4)}{\Sigma_{i=1}^{n} x_i^4}, \tag{30}$$

The W_{ij}^4 weights are adjusted using back propagation,

$$\delta_j^4 = \left(d_j^4 - O_j^4\right), \tag{31}$$

$$W_{ij}^4(k+1) = W_{ij}^4 + \eta w.\delta_j^4(k).x_i^4(k) + \alpha w.\Delta W_{ij}^4(k), \tag{32}$$

where δ_j^4 is the error signal, d is the desired output, and the o is the plant output. Where η_m and αw are the learning rates and the momentum parameter for adjusting W_{ij}^4 respectively.

4. Simulation Results

Investigating stability, security and smooth transfer of energy between connected regions. The stability analysis uses control strategies such as PI and AFLN controls. The results of the simulation shall be evaluated by the PI controller and the AFLNN controller as complementary controllers. The proposed controller addresses the non-linearity of synchronous generators under 3ϕ – g fault conditions by running simulations for 24 hours. At t=16 hours, a fault occurs for 36 seconds on bus 27. At night, the household load decreases because of lower electricity consumption, while at t=6 hours, the household load increases by 10.75 MW compared to the previous value. This increase in load induces small oscillations in the system which gradually increases over time.

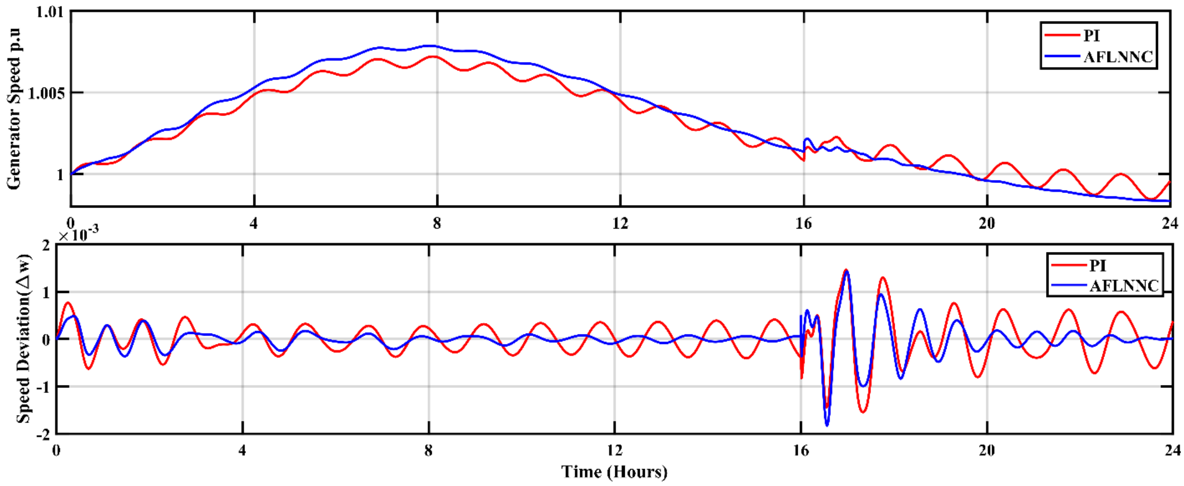

Fig. 4 *Generator speed and the speed deviation*

The Fig 4 explains the simulation of PI controller as a supplementary controller to maintain the generator speed at 1p.u. Although the generator speed is maintained at unity, when the fault occurs at 16 hours the generator speed deviation is increased, and these oscillations do not damp for 24 hours simulation. The proposed controller effectively maintain the generator speed during fault and the generator speed deviation damps effectively after fault.

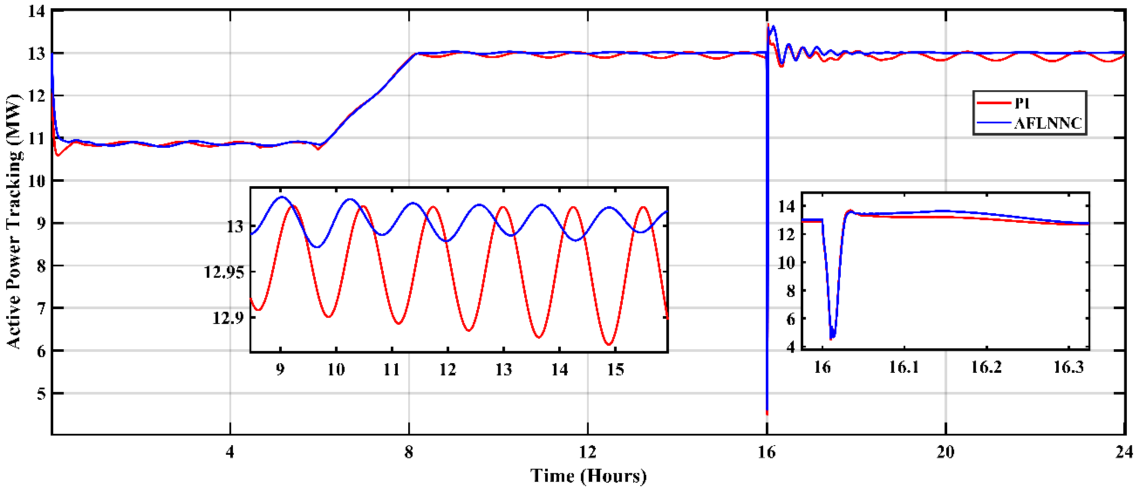

Fig. 5 *Active power tracking at GUPFC bus*

At the beginning, the power level is maintained at a steady 10.75 MW. At t=6 hours, an increase in load leads to a rise in demand for active power. The GUPFC adjusts the line voltage magnitude and angle (v∠δ) as well as the line reactance to enhance active power flow in the system. With the rise in load, the power demand grew from 10.75 MW to 13 MW, as shown in Fig 5. The PI controller demonstrates an oscillatory response while following the active power demand. In contrast, AFLNNC experiences fewer oscillations, and the proposed controller significantly reduces power fluctuations, enabling more stable system performance. Excessive power flow during a fault can threaten system stability; however, the proposed controller effectively mitigates the fault in accordance with grid code standards.

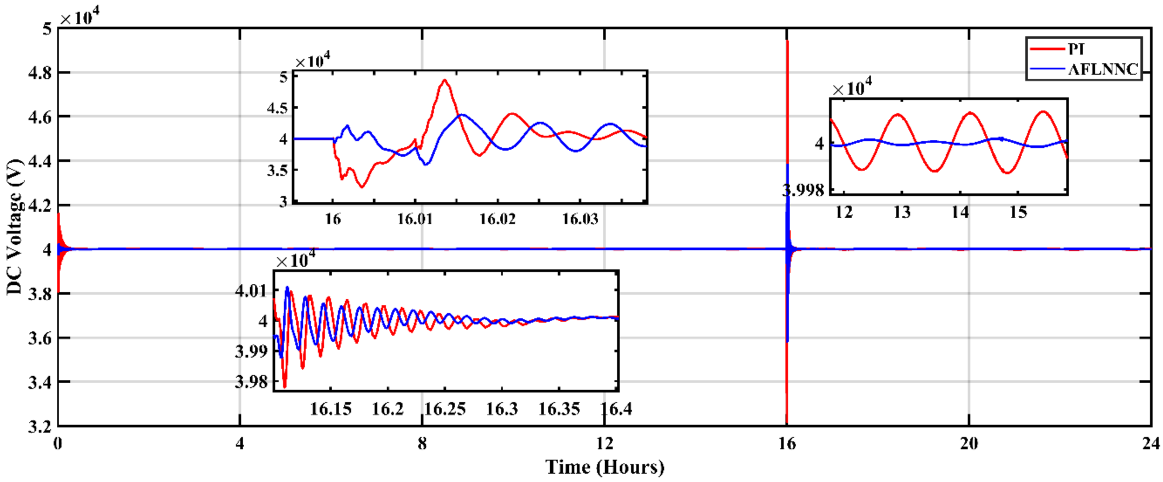

Fig. 6 *DC-link voltage across the GUPFC capacitor under PI and AFLNNC control schemes*

In the modeling section, it was explained that VSC2 and VSC 3 converters are connected via DC link capacitor through VSC 1 converter to facilitate smooth power transfer. During three-phase fault conditions, when the PI is used as a supplementary controller. The performance of the PI controller in damping the DC voltage fluctuations is not satisfactory, whereas the proposed controller effectively minimizes the oscillations in DC voltage and prevents them from escalating within the system, as illustrated in Fig 6.

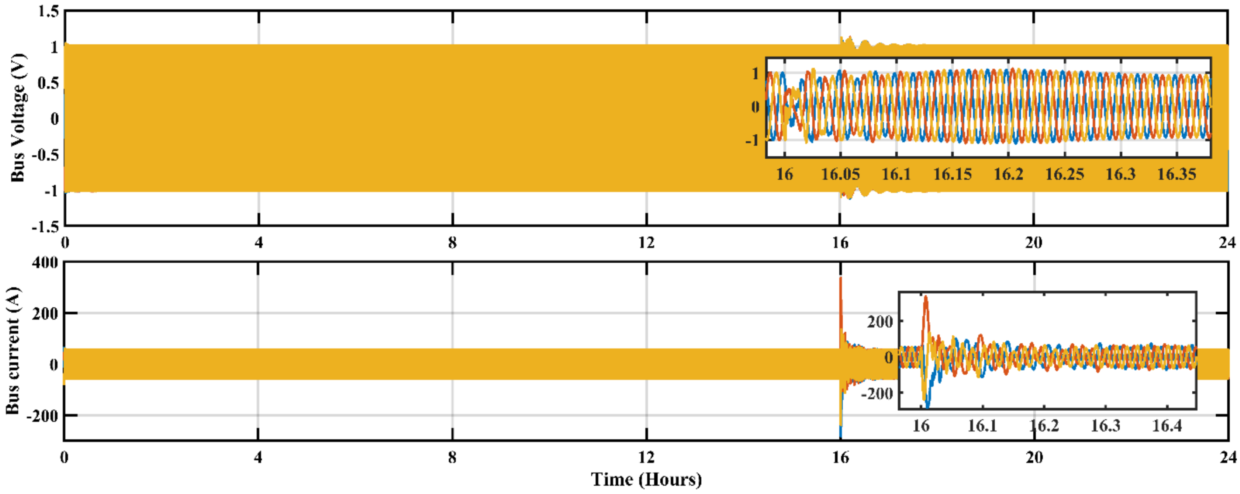

Fig. 7 *Three phase bus voltage at MTL load bus*

The Fig. 7 shows the $3\varphi - g$ fault MTL bus voltage and current. Before fault the bus voltage is maintained at 1 and -1 during fault the voltage magnitude is reduced to 0.5, as soon as the fault is cleared, voltage is restored back to 1 p.u. The current MTL bus is maintained at 1.5 p. u but during fault, excessive current passes through the bus load. The proposed controller effectively damps the current fluctuations and monitor the current and does not let them grow again.

Table 2 *Summary of conventional and proposed controlle performance Indices*

Performance Metric	PI Controller	AFNNC Controller	Observation
Speed Response	Smooth rise Small oscillations deviation higher near fault t=16H	Faster rise, better damping, lower oscillations	AFNNC shows improved damping and reduced oscillations compared to PI
Speed Deviation ($\Delta\omega \times 10^{-3}$)	±2 peak oscillations, more fluctuation's post-fault (16 h)	Lower oscillations, faster stabilization	AFNNC minimizes deviation and enhances dynamic stability
Active Power Tracking (MW	Does not exactly track 10.75 MW, slower adjustment, larger dip during fault (16 h)	Faster adjustment to 13 MW, quicker recovery from dip	AFNNC provides better tracking accuracy and faster recovery
Disturbance Rejection	Slower recovery; oscillatory during fault	Quicker recovery; stable with reduced oscillations	AFNNC superior in fault handling
Overall Performance	Acceptable but with higher oscillations and slower fault recovery	Robust, fast, and stable under both normal and faulty conditions	AFNNC outperforms PI

The performance of proposed controller and conventional controller is compared in Table 2. The system's dynamic response was assessed using key performance indicators, including generator speed. speed deviation, voltage stability, active power tracking and DC voltage across GUPFC capacitor under $3\varphi - g$ fault case. The proposed model shows strong agreement with previously reported findings, supporting the accuracy and reliability of the model in [28], [29], [30]. The proposed simulations were conducted in MATLAB/Simulink over an extended duration of 2400 hours and were compared with those reported in earlier studies. The proposed model is highly nonlinear and in earlier studies only ran simulations for a few seconds or for few minutes, that's all they managed. Our comparison indicates that the proposed method suppresses low-frequency oscillations more rapidly and maintains higher stability margins, even under three-phase fault conditions. These outcomes are consistent with the performance characteristics observed in existing control strategies. Small differences in the numbers usually come from changes in system setup, parameter choices, or how we model the system.

5. Conclusion

In conclusion, this study highlights the effectiveness of combining an Adaptive Fuzzy Logic Neural Network Controller (AFLNNC) with a Generalized Unified Power Flow Controller (GUPFC) for mitigating low-frequency oscillations in smart grids with high renewable energy penetration. By integrating the rule-based reasoning of fuzzy logic with the adaptive learning capabilities of neural networks, the proposed controller provides a flexible and intelligent control solution. A key advantage of this approach is its ability to handle operating point variations, parameter uncertainties, and nonlinear system dynamics without relying on an exact mathematical model of the power system. This feature makes the controller particularly well-suited for modern smart grids, where the variability and complexity introduced by renewable energy sources pose significant challenges to system stability.

Analysis of time-domain simulations shows that the AFLNNC-based GUPFC performs better dynamically in both faulted and steady-state scenarios. When compared to a traditional proportional-integral (PI) controller, improvements are seen in the accuracy of active power tracking, speed deviation ($\Delta\omega$), and generator speed response. The suggested controller has a less noticeable transient dip, faster post-fault recovery, and less overshoot and undershoot during a three-phase fault (3φ-gfault). Better tracking and disturbance rejection performance are indicated by active power being kept closer to its reference value. Additionally, the suggested control scheme greatly improves DC-link voltage regulation, which boosts converter stability.

In general, the proposed smart grid system results indicate that, relative to the traditional PI control method, the proposed AFLNNC-based control approach has stronger damping, robustness, and dynamic resilience. In the case of low inertia and high penetration of renewable energy sources and converter-based generation, the dynamic and structural flexibility of the proposed control approach ensures reliable performance. Moreover, the coordinated active and reactive power control of the GUPFC enhances the fault ride-through capability, voltage profile, and stability of inter-area power transfer. Based on the above findings, the proposed intelligent control approach can be considered an effective means to enhance operational reliability and stability in modern renewable energy-integrated power systems, thus accelerating the transition towards sustainable low-inertia smart grid infrastructure.

Acknowledgement

Universiti Tun Hussein Onn Malaysia (UTHM) provided the research facilities for this study. A special thank you is required for the technical assistance section provided by the Advanced Control in Power Converter research group at UTHM and MAHSA University.

Conflict of Interest

Regarding the publication of the paper, the authors declare that they have no conflicts of interest.

Author Contribution

The authors confirm contribution to the paper as follows: ***study conception and design:*** *Nadia Zeb, Shamsul Aizam Zulkifli;* ***data collection:*** *Nadia Zeb, Shamsul Aizam Zulkfli;* ***analysis and interpretation of results:*** *Nadia Zeb, Shamsul Aizam Zulkifli, Muhammad Syazmie Sepeeh, Nedim Tutkun, Noor Hisyam Ibrahim;* ***draft manuscript preparation:*** *Nadia Zeb, Shamsul Aizam Zulkifli, Muhammad Syazmie Sepeeh, Nedim Tutkun, Noor Hisyam Ibrahim*

References

[1] Mehrzad A, Mehrzad, A., Darmiani, M., Rouhani, S. H., Su, C.-L., Sepestanaki, M. A., Mofidipour, E., Monti, A., & AnvariMoghaddam, A. (2026). Inertia in Renewable Power Systems: A Review of Estimation Methods and Practical Implementation. Renewable & Sustainable Energy Reviews, 226(Part A), 1-16. Article 116246. https://doi.org/10.1016/j.rser.2025.116242.

[2] Gao H, Xin H, Huang L, Ma F., Leng R., & Yang Y., (2025) Inverse Distribution of Inertia and Damping for Mitigating Low-Frequency Oscillations in Power Systems. IEEE Transactions on Power Systems, vol. 40, no. 4, pp. 3388-3400, doi: 10.1109/TPWRS.2025.3527204

[3] Saadatmand M, Gharehpetian GB, Siano P, Alhelou HH (2021) PMU-Based FOPID Controller of Large-Scale Wind-PV Farms for LFO Damping in Smart Grid. IEEE Access, vol. 9, pp. 94953-94969, doi: 10.1109/ACCESS.2021.3094170

[4] Ahsan F, Dana NH, Sarker SK, Li L., Muyeen M. S., Ali F. M., Tasneem Z., Hasan M. M., Abhi H. S., Islam R. M., Ahamed H. M., Islam M. M,, Das K. S., Badal R. F. M., & Das. P., (2023) , Data-driven next-generation smart grid towards sustainable energy evolution: techniques and technology review. Prot Control Mod Power Syst 8, 43. https://doi.org/10.1186/s41601-023-00319-5

[5] Im, S., Lee, K., Lee, B. (2024), Estimation of maximum non-synchronous generation of renewable energy in the South Korea power system based on the minimum level of inertia. IET Renew. Power Gener.18, 1260–1268. https://doi.org/10.1049/rpg2.12964

[6] Saeed M.H., Fangzong W., Kalwar B.A., Iqbal S. (2021), "A Review on Microgrids' Challenges & Perspectives, IEEE Access, vol. 9, pp. 166502-166517, 2021, doi: 10.1109/ACCESS.2021.3135083 9

[7] Alatai, S., Salem, M., Ishak, D., Das, H. S., Alhuyi Nazari, M., Bughneda, A., Kamarol, M. (2021). A Review on State-of-the-Art Power Converters: Bidirectional, Resonant, Multilevel Converters and Their Derivatives. Applied Sciences, 11(21), 10172. https://doi.org/10.3390/app112110172

[8] V. Mahajan, (2008) "Power System Stability Improvement with Flexible A.C. Transmission System (FACTs) Controller," 2008 Joint International Conference on Power System Technology and IEEE Power India Conference, New Delhi, India, pp. 1-7, doi: 10.1109/ICPST.2008.4745204.

[9] Mandal A, Muttaqi K.M., Islam M.R., Sutanto D. (2025).A novel architecture of the solid-state unified power flow controller and its integration into the power grid, Electric Power Systems Research, Volume 241, 111296, https://doi.org/10.1016/j.epsr.2024.111296.

[10] Abasi M., Joorabian M., Saffarian A., Seifossadat S.G., (2022). An algorithm scheme for detecting single-circuit, inter-circuit, and grounded double-circuit cross-country faults in GUPFC-compensated double-circuit transmission lines. Electr Eng 104, 2021–2044 . https://doi.org/10.1007/s00202-021-01440-0

[11] S. Zarrabian,(2019). Hybrid Analysis for Damping Inter-Area Oscillations Using GUPFC in Power Systems, 2019 IEEE Power & Energy Society General Meeting (PESGM), pp. 1-5, doi: 10.1109/PESGM40551.2019.8974075.

[12] Solomon, E., Khan, B., Boulkaibet, I., Neji, B., Khezami, N., Ali, A., Mahela, O. P., & Pascual Barrera, A. E. (2023). Mitigating Low-Frequency Oscillations and Enhancing the Dynamic Stability of Power System Using Optimal Coordination of Power System Stabilizer and Unified Power Flow Controller. Sustainability, 15(8), 6980. https://doi.org/10.3390/su15086980

[13] Sadiq R, Wang Z, Chung CY (2023). A multi-model multi-objective robust damping control of GCSC for hybrid power system with offshore/onshore wind farm, International Journal of Electrical Power & Energy Systems, Volume 147, 108879, https://doi.org/10.1016/j.ijepes.2022.108879.

[14] Bento MEC (2022). A Hybrid Particle Swarm Optimization Algorithm for the Wide-Area Damping Control Design, IEEE Transactions on Industrial Informatics, vol. 18, no. 1, pp. 592-599, doi 10.1109/TII.2021.3054846.

[15] Li S, Alanazi M, Abdulkader R, Salem M., Abdolrasol G.M. M., Mohamed A. F., Alghamdi A.H.T., (2024) Improving the time delay in the design of the damping controller with the aim of improving the stability of the power system in the presence of high penetration of renewable energy sources, International Journal of Electrical Power & Energy Systems, Volume 158 , 109922, https://doi.org/10.1016/j.ijepes.2024.109922

[16] Messaoud, F. Z. ., Tedjini, H., Hazzab, A., Abasi, M., & Meslem, Y., (2021). A Novel and Robust Model of the GUPFC Controller System Based on Adaptive Fuzzy Logic- PI Controller to Enhance the Control System Performance in Following Reference Active and Reactive Power. International Journal of Integrated Engineering, 13(4), 51-62 , https://publisher.uthm.edu.my/ojs/index.php/ijie/article/view/7234

[17] Yao Q, Zeng Y, Jia Q (2023) A Novel Non-Isolated Cubic DC-DC Converter with High Voltage Gain for Renewable Energy Power Generation System, Energy Engineering, Volume 121, Issue 1 ,Pages 221-241, https://doi.org/10.32604/ee.2023.041028.

[18] Makula CS, Kumar A (2022), GUPFC Impact in Managing the Congestion Using Generation Rescheduling. In: Kumar, A., Srivastava, S.C., Singh, S.N. (eds) Renewable Energy Towards Smart Grid. Lecture Notes in Electrical Engineering, vol 823. Springer, Singapore. https://doi.org/10.1007/978-981-16-7472-3_27

[19] Binkowski T, Szcześniak P., (2024), Independent Control of Active and Reactive Power Flow for a Single-Phase, Unidirectional Onboard Power Converter Connecting the DC Power Bus to the AC Bus. Energies, 17 (2), 540. https://doi.org/10.3390/en17020540

[20] Brezovec M, Kuzle I, Krpan M (2022), Detailed mathematical and simulation model of a synchronous generator. Journal of Energy -Journal of Energija, 64:. https://doi.org/10.37798/2015641-4147

[21] Zhang X.P., Handschin E., Yao M. (2001), Modeling of the Generalized Unified Power Flow Controller (GUPFC) in a nonlinear interior point OPF, IEEE Transactions on Power Systems, vol. 16, no. 3, pp. 367-373, Aug., doi: 10.1109/59.932270

[22] Sharma, S., Vadhera, S., (2020), Mathematical modelling and application of Generalized Unified Power Flow Controller (GUPFC) steady state model for power system network. Journal of Information and Optimization Sciences, 41(1), 119–128. https://doi.org/10.1080/02522667.2020.1721590

[23] PPham, D.-A., & Han, S.-H. (2023). Designing a Ship Autopilot System for Operation in a Disturbed Environment Using the Adaptive Neural Fuzzy Inference System. Journal of Marine Science and Engineering, 11 (7), 1262. https://doi.org/10.3390/jmse11071262

[24] Garcia-Trevino E.S., Yang P., Barria J.A., (2024), Wavelet Probabilistic Neural Networks, IEEE Transactions on Neural Networks and Learning Systems, vol. 35, no. 1, pp. 376-389, doi: 10.1109/TNNLS.2022.3174705.

[25] Ahmad I, M'zoughi F, Aboutalebi P, Garrido I., Garrido J.A., (2023), Fuzzy logic control of an artificial neural network-based floating offshore wind turbine model integrated with four oscillating water columns, Ocean Engineering, Volume 269, 113578, https://doi.org/10.1016/j.oceaneng.2022.113578.

[26] Moody J, Darken C.J., (1989),Fast Learning in Networks of Locally-Tuned Processing Units. Neural Comput 1 (2): 281–294. doi: https://doi.org/10.1162/neco.1989.1.2.281

[27] Lin C.J, Jhang J.Y (2022), Intelligent Traffic-Monitoring System Based on YOLO and Convolutional Fuzzy Neural Networks," in IEEE Access, vol. 10, pp. 14120-14133, 2022, doi: 10.1109/ACCESS.2022.3147866

[28] Jafari M, Gharehpetian G.B, Anvari-Moghaddam A (2026), Adaptive fuzzy logic-based coordinated tuning of distributed virtual synchronous generators parameters for frequency oscillation suppression in islanded microgrids, Electric Power Systems Research, Volume 254, 112656 https://doi.org/10.1016/j.epsr.2025.112656.

[29] Ding Y, Zhao K, Duan J, Sun L (2026), Low-Frequency Oscillation Suppression Strategy for Ship Microgrid Based on Virtual PSS Adaptive Damping Control with Supercapacitor. Electronics, 15 (2), 390. https://doi.org/10.3390/electronics15020390

[30] Sah CK, Kannan AS (2025) Sah, C. K., & A.S, K. (2025). Performance Analysis of Various FACTS Devices Incorporated in Power System Damping Controllers. International Research Journal of Multidisciplinary Technovation, 7(6), 129–150. https://doi.org/10.54392/irjmt2568